

In situ growth of Ag nanoparticles on α - Ag_2WO_4 under electron irradiation: probing the physical principles

Miguel A San-Miguel^{1,7}, Edison Z da Silva², Sonia Zanetti³, Mario Cilense³, Maria T Fabbro⁴, Lourdes Gracia⁵, Juan Andrés⁵ and Elson Longo⁶

¹Institute of Chemistry, State University of Campinas—Unicamp, 13083-970, Campinas, SP, Brazil

²Institute of Physics ‘Gleb Wataghin’, State University of Campinas—Unicamp, 13083-970, Campinas, SP, Brazil

³Institute of Chemistry, UNESP (Universidade Estadual Paulista), 14800-900 Araraquara, SP—Brazil

⁴Chemistry Department, Federal University of Sao Carlos—UFSCar, 13565-905, São Carlos—SP—Brazil

⁵Departament de Química Física i Analítica, Universitat Jaume I, Castellón E-12071, Spain

⁶INCTMN-UNESP, Universidade Estadual Paulista, PO Box 355, CEP 14801-907 Araraquara, SP, Brazil

E-mail: smiguel@iqm.unicamp.br, zacarias@ifi.unicamp.br, zanetti@iq.unesp.br, mcilense@iq.unesp.br, mariaterazafabbro@gmail.com, Igracia@qfa.uji.es, andres@qfa.uji.es and elson.liec@gmail.com

Received 6 January 2016, revised 29 March 2016

Accepted for publication 12 April 2016


Published DD MM 2016



CrossMark

Abstract

Exploiting the plasmonic behavior of Ag nanoparticles grown on α - Ag_2WO_4 is a widely employed strategy to produce efficient photocatalysts, ozone sensors, and bactericides. However, a description of the atomic and electronic structure of the semiconductor sites irradiated by electrons is still not available. Such a description is of great importance to understand the mechanisms underlying these physical processes and to improve the design of silver nanoparticles to enhance their activities. Motivated by this, we studied the growth of silver nanoparticles to investigate this novel class of phenomena using both transmission electron microscopy and field emission scanning electron microscopy. A theoretical framework based on density functional theory calculations (DFT), together with experimental analysis and measurements, were developed to examine the changes in the local geometrical and electronic structure of the materials. The physical principles for the formation of Ag nanoparticles on α - Ag_2WO_4 by electron beam irradiation are described. Quantum mechanical calculations based on DFT show that the (001) of α - Ag_2WO_4 displays Ag atoms with different coordination numbers. Some of them are capable to diffuse out of the surface with a very low energy barrier (less than 0.1 eV), thus, initiating the growth of metallic Ag nanostructures and leaving Ag vacancies into the bulk material. These processes increase the structural disorder of α - Ag_2WO_4 as well as its electrical resistance as observed in the experimental measurements.

 Online supplementary data available from stacks.iop.org/NANO/0/000000/mmedia

Keywords: α - Ag_2WO_4 , Ag nanoparticles, transmission electron microscopy, density functional theory, plasmonic effect

SQ1 (Some figures may appear in colour only in the online journal)

Introduction

Electrons show dual wave-particle behavior. During the last few years, it has been well established that the electron beams

⁷ Author to whom correspondence should be addressed.

generated by a transmission electron microscope or a scanning electron microscope are very powerful tools for the atomic-scale characterization of structure, chemical composition, and the electronic properties of materials [1–6]. Further, the use of such electron beams allows precise control at the nanoscale or single nanoparticle (NP) level. Transmission electron microscopy (TEM) is based on the interaction of an electron beam with the material under examination, and interesting phenomena often occur due to the electron-solid interactions as observed during imaging [7]. Furthermore, useful insights have been obtained from existing understanding of the interaction of electron beams with solid matter [8].

Bombardment of solids with high-energy electrons leads to novel phenomena, many of which have been discovered in the process of making TEM measurements. For example, nanoscale crystallization and growth processes that only occur in the presence of the electron beam [9–14]. Other examples of materials for which structural changes have been observed under irradiation by an electron beam include the nanoscale phase/shape transformation [15, 16] that is observed on Au nanoparticles [17], metal oxide nanoparticles [18], silicon oxide nanowires [19], and lead iodide nanoparticles [20], and the morphological and structural evolution of WS₂ nanosheets [21]. Also, other phenomena such as the modification of inorganic nanostructures [22], formation of nanorods and particles [23], and nanostructure fabrication [24] and coalescence [25] can occur. All these processes are essentially different from such as ion bombardment techniques inducing the formation of nanostructures [26, 27].

At the nanoscale, electrons also induce local reactions in adsorbed functional molecules. It has been shown that these electron beam induced processes can be performed on almost any kind of substrate [28]. Recently, Bohler *et al* [29] reviewed low-energy, electron-initiated molecular syntheses and their applications in the modification of surfaces. In summary, irradiation of materials with an electron beam in a TEM can be used to fabricate nanomaterials and to investigate their morphology, structure, and chemical transformations. This is important for the development of novel nanostructures, especially for materials that cannot be fabricated using conventional chemical and physical methods. On account of these so-called localized surface plasmon resonances (LSPRs), NPs show intense light absorption and scattering due to a near-field enhancement because of their nanoscale confinement [30–32]. Semiconductor nanocrystals gain their optical properties from excitonic quantum confinement, which leads to particle-in-spherical-box like energy levels [33]. However, unlike this idealized model, the surface forms a finite potential barrier of the stoichiometric semiconductor lattice core, resulting in wave function leakage [34].

One of the main goals in NP research is to obtain noble metal NPs, such as gold or silver, that exhibit LSPRs at optical frequencies [35, 36], and to manipulate the potential barrier and leakage. The ability to do this would increase the range of applications of these materials in many fields, ranging from photovoltaics to bioimaging [37–40]. Recently, this

effect has been discussed concerning semiconductor nanocrystals [41, 42]. Desirable electrical and optical properties of novel metal nanoparticles can be achieved by tailoring their size, shape, and morphology [43]. However, synthetic methods to achieve this have yet to be developed. In this context, electron beam irradiation has great potential for the preparation of noble and transition metal NPs [44, 45]; for example, the synthesis of Ag nanoparticles by electron beam irradiation has been reported by Rani *et al* [46].

Although recent advances in *in situ* electron microscopy techniques have allowed direct observation of the growth of colloidal nanocrystals [47–50], giving insights into its mechanism, less attention has been paid to the atomistic description of this effect induced by the irradiation of electrons. Primarily, this is because these phenomena occur too rapidly to be detected on the nanocrystal surfaces. Very recently, using an electron beam in an electron microscope under high vacuum, we identified the formation and growth of Ag nanoparticles on α -Ag₂WO₄ [51–57], β -Ag₂WO₄ [58], β -Ag₂MoO₄ [59, 60], and Ag₃PO₄ [61], and other authors have also reported interest in these fascinating systems [62–71]. Much of the applications of the aforementioned Ag materials are based on their photoluminescence properties [54] and bactericidal/antibacterial effect (which allows their use in clinical sterilization) [55].

Our understanding of the new and interesting phenomena that occur on nanocrystal surfaces remains in its infancy. The lack of systematic information about these phenomena has prompted us to explore trends in the formation of Ag NPs. Consequently, in the present work, our target is to understand the physical principles behind the formation of Ag NPs on α -Ag₂WO₄ caused by electron beam irradiation. Using theoretical analysis in the form of density functional theory (DFT) calculations and *ab initio* molecular dynamics simulations, along with the experimental observations, we have attempted to understand the described phenomena under experimental conditions. Our investigations have provided atomistic insights into the electronic and structural localization of plasmonic behavior. Also, our investigation indicates that the injected electrons survive longer by being captured at sites localized near the surface. These sites have all the characteristics required to be active sites in plasmonic applications.

This paper is organized as follows: in the methods section, the theoretical procedures and computational methods, as well as the experimental aspects of the synthesis, structural, optical and morphological characterization, are described; the results section is used to present and discuss the results; and the conclusions section provides a summary of this work and concluding remarks.

Methods

Theoretical methods and model systems

Electronic structure calculations using DFT were performed for the α -Ag₂WO₄ system using the VASP code [72–74].

Plane waves were used to describe the valence electrons and the inner electrons were treated using the projector augmented wave (PAW) method [75, 76]. The valence states that were explicitly included in the calculation were 4d and 5s (11 electrons) for Ag atoms, 5d and 6s (6 electrons) for W atoms, and 2s and 2p (6 electrons) for O atoms. All other electrons were considered as core electrons with their densities frozen as in the reference used to extract the PAW potential. A kinetic energy cutoff of 460 eV was used for the plane wave expansion for all systems, which was adequate to obtain total energies converged to at least 1 meV/atom.

Sampling of the Brillouin zone was performed using the Monkhorst–Pack method with different k -points grids according to the system size. Therefore, for the analysis of the electronic structure, the number of k -points was tested with respect to the geometry optimization process. The tetrahedron method with Blöchl corrections [77] was also used. All calculations were non spin-polarized.

Exchange and correlation effects were treated using the generalized gradient approximation using the Perdew–Burke–Ernzerhof density functional [78, 79]. The conjugate gradient method was used to perform energy minimization to obtain the relaxed systems. Atoms were considered fully relaxed when the Hellmann–Feynman forces converged to less than 0.005 eV Å⁻¹ per atom.

Selected structures were also studied using *ab initio* molecular dynamics simulations in the canonical ensemble at 300 K. The time step was 3 fs, and a typical simulation spanned about 3 ps.

Minimum energy pathways for the diffusion process of Ag atoms from positions in the first slab layer to outer sites on the surface were investigated using the nudged elastic band (NEB) method. Both the initial and final configurations were previously optimized. Subsequently, four intermediate configurations were generated by linear interpolation between the initial and end points. These intermediate configurations were relaxed under NEB constraints in which the ions were connected by springs to keep them equidistant from neighboring configurations. More details of the NEB method can be found in [80].

Experimental

Synthesis

α -Ag₂WO₄ nanoparticles were synthesized via a co-precipitation reaction in aqueous media. Firstly, two aqueous solutions were prepared by adding, separately, a silver salt (2 mmol, AgNO₃; 99.8% purity, Sigma-Aldrich) and a salt of tungstate (1 mmol, Na₂WO₄·2H₂O; 99.5% purity, Sigma-Aldrich) to two portions of distilled water. Then, the silver solution was added dropwise to the stirred tungsten solution at 90 °C for 30 min. The α -Ag₂WO₄ precipitate was filtered and washed several times with distilled water, and dried at 60 °C for 24 h.

The α -Ag₂WO₄ microcrystals and the formation of Ag nanofilaments were observed using a field-emission scanning

electron microscopy (FE-SEM) instrument model Supra 35-VP, Carl Zeiss, Germany operated at 15 kV.

Fabrication set-up for electric transport property measurements

A non-conducting gap was made on an indium tin oxide (ITO) glass by scratching the conductive surface, separating it into two pieces. Thus, each piece was used as an electrode. The as-synthesized α -Ag₂WO₄ nanoparticles were mixed into a paste with isopropanol. This paste was poured on the surface of the gap between the two electrodes. After drying in air at room temperature, the ITO glass with the thick film covering was isostatically pressed at 300 MPa to increase the adhesion of the film to the gap. This led to a thick film of α -Ag₂WO₄ nanoparticles that covered the gap between the two ITO pieces. The electrode was dried overnight at 70 °C and then stored in a low humidity environment (using silica gel) until variable time electron beam irradiation was carried out in a scanning electron microscope.

I - V measurements of the thick film (Keithley 2400 Source Meter), before and after exposure to electron beam, were carried out at room temperature at 30 kV for 5, 10, 20, 40, and 60 min. To avoid external environmental influences, all measurements were carried out in a closed cell filled with silica gel so that the humidity level was low. The electrical resistance was calculated from the slope of the I - V curve. The experimental device is schematically shown in the inset of figure 4 and in the supplementary material.

Results and discussion

α -Ag₂WO₄ crystals, the object of the present study, have been studied previously both experimentally and theoretically [50–55].

The formation of Ag nanostructures when α -Ag₂WO₄ crystals are irradiated with an electron beam becomes evident using time-resolved FE-SEM techniques. Figure 1 shows two images extracted from a real time movie included in the supplementary material.

In the present article, we studied theoretically in detail one of the most stable surfaces of α -Ag₂WO₄: the (001) surface, and, this surface has been studied by TEM and x-ray diffraction experiments previously [81].

In previous studies, the geometrical and the electronic structure of the (100) surface were modeled using a three-layer model [54]. In this work, we used a similar strategy to generate a super-cell model for the (001) surface at low computational cost. Thus, we combined geometry optimizations along with *ab initio* molecular dynamics simulations for two supercells of 11.234 × 12.574 Å area with three and six layers, respectively. We found that after relaxation, the surfaces were significantly different from those of the just-cleaved planes. Because both the three and six-layer models reproduced this effect, to reduce computational costs all further calculations were carried out using three layers. The cleaved surface was relaxed by electronic structure relaxation

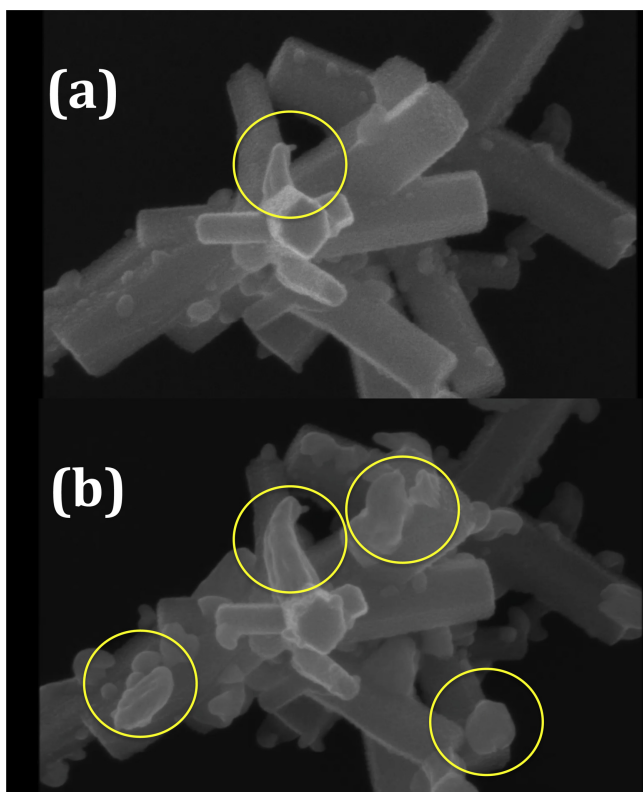


Figure 1. *In situ* FEG-SEM images of α - Ag_2WO_4 crystals at (a) time zero (after a rapid approach and focus adjustment) and (b) 5 min. The formation of Ag nanostructures is highlighted with yellow circles.

and a new reconstructed geometry was obtained. Figure 2 shows the two slabs, the cleaved surface, (a), and the reconstructed structure, (b). Figure 2 and table 1 show that there are eight Ag surface atoms with coordination numbers (CN) ranging from 2 to 6 (see table 1). The CNs of the cleaved surface are different to those of the reconstructed surface. The CNs of the Ag atoms in the reconstructed surface (figure 2(b)) correlate with their surface height, as can be seen in table 1. Thus, the atoms Ag-7 and Ag-8 that are further out from the surface are those with the lowest CNs: 2 and 3, respectively, whereas the atoms in the interior have higher CNs (from 4 to 6) more like those of the atoms in the bulk.

This structural rearrangement suggests that the (001) surface can be understood in terms of an assembly of corner-sharing Ag clusters, as shown in the middle panel of figure 2. This is distinct from that of the (100) surface that was studied previously [52]. In that model, only Ag atoms with CNs of 4 and 6 were found. Even more generally speaking, these α - Ag_2WO_4 systems can be seen as metal oxides with a structure based on exposed Ag clusters whose geometries change slightly in response to external effects. Hence, pressure fluctuations or the presence of different solvents and molecular adsorption might significantly alter the arrangement of the surface clusters and, consequently, the surface stability.

Another external factor that could affect the surface structure is electron injection. In particular, upon electron bombardment, the α - Ag_2WO_4 crystals show Ag nucleation at

the surfaces. Clearly, this is a surface induced effect that occurs first with the rearrangement of some Ag clusters, followed by the diffusion of Ag atoms from the interior of the crystal to form the observed Ag NPs at the surface.

Therefore, our first aim was to understand possible routes for the diffusion of the Ag atoms from the bulk material to the surface, in particular, for those Ag atoms closer to the surface. The energy barrier for the movement of the outmost Ag atom out of the surface has been calculated using the NEB method. In addition to the NEB calculations, to find the stability of Ag atoms in their final position outside the surface, we performed geometry optimizations on the system after displacing one Ag atom to a position outside the surface. This procedure was done for each of the eight Ag surface atoms in the supercell. Only two Ag atoms, referred to as Ag-4 and Ag-5, found stable positions outside the surface, while the others returned to their original positions. Therefore, we performed NEB calculations for atoms Ag-4 and Ag-5.

Figure 3 shows images of the evolution of Ag-4 from its surface position (I-00) to its final stable position (I-05). It also shows the energy profile along with the position of the moving atom. A low value for the energy barrier of 0.08 eV was found, indicating that Ag-4 atom is very mobile. Figure 4 shows the same process for the Ag-5 atom; again it shows the evolution of the Ag-5 atom from I-00 to I-05, similar to Ag-4. The movement of Ag-5 has an energy profile with a minimum at I-01 and a total energy barrier of 0.05 eV, even smaller than that of Ag-4. These NEB calculations show that, in these two cases, the Ag atoms are loosely bound and are excellent candidates to initiate the diffusion of atoms out of the surface to form the experimentally observed Ag NPs and nanorods. Another interesting aspect arises from the analysis of the electron density distribution based on the computed Bader charges. These show that Ag-4 and Ag-5 gain charges of 0.12 and 0.31 e^- , respectively, on moving along the diffusion pathway; therefore, their diffusion is accompanied by reduction.

The formation of Ag NPs observed in the accompanying experiments is triggered by the injection of electrons from the electron microscope. Previous studies have shown that the process is not actually dependent on the energy of the incoming electrons and is, instead, associated with exposure time [52]. Therefore, we argue that the loose surface Ag atoms gain the necessary energy to diffuse from the surface from impact with the incoming electrons.

We have also carried out calculations of the electron injection process, including the effect of additional electrons on the structure of the surface slab. Thus, we have verified that the addition of between 1 to 4 electrons did not significantly alter the geometry of the surface as illustrated in the Supplementary Material. Our results, and those of previous theoretical studies, indicate that some Ag surface atoms can migrate to positions above the surface, and this is a possible mechanism for the formation of Ag clusters and NPs at the surfaces provoked by the electron irradiation. As a consequence, Ag vacancies [V_{Ag}^+] are formed in the bulk solid, contributing to disorder. This disorder has clear consequences on the conductivity of α - Ag_2WO_4 . Also, upon further

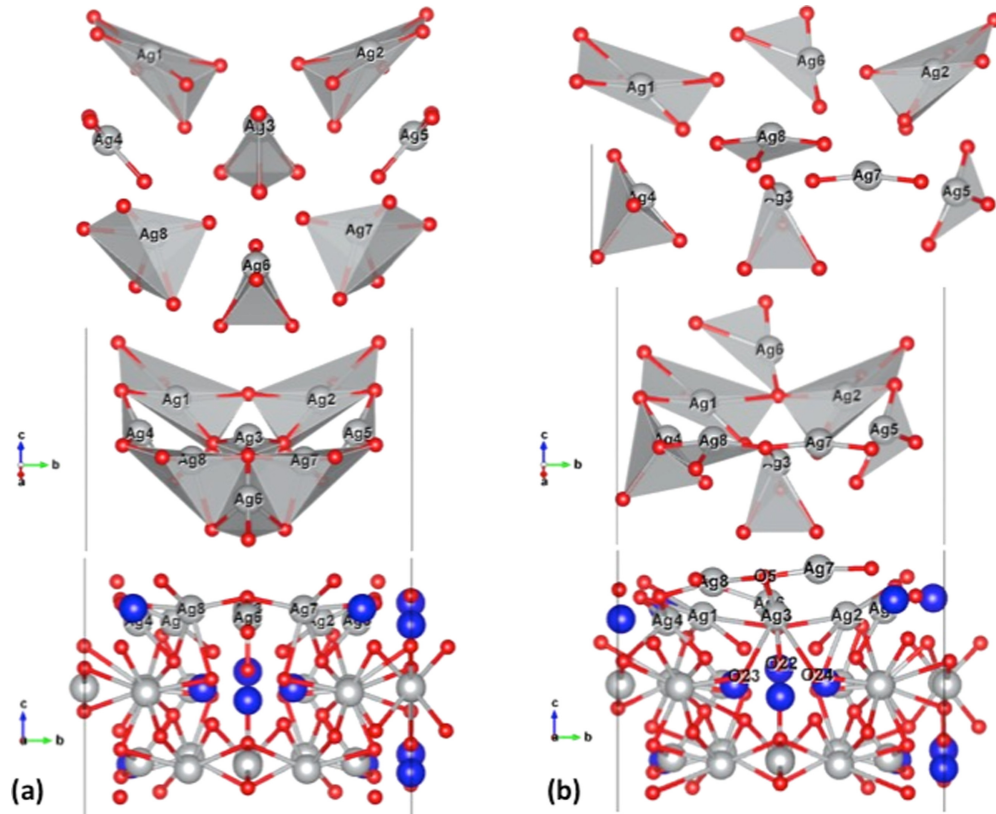


Figure 2. The α - Ag_2WO_4 (001) surface (a) generated from the bulk after cleaving and (b) after the relaxation process. The bottom panels show lateral views of the three-layer slab in ball-and-stick view. Ag, W, and O atoms are colored in gray, blue, and red, respectively. The middle panels show a polyhedral model of the top layer slab rotated by 30° to assist viewing. A detail of each AgO_x polyhedron is shown in the top panel.

Table 1. Coordination number (CN) and relative heights (z -distance) respect to the lowest Ag atom for the outmost external Ag atoms in the supercell for the unreconstructed (Z1) and reconstructed (Z2) surfaces.

Atom	(001)		Reconstructed (001)		
	CN	Z1	CN	Z2	Z1-Z2
Ag-1	6	0.010	5	0.181	0.051
Ag-2	6	0.008	6	0.199	0.071
Ag-3	4	0.474	4	0.192	-0.402
Ag-4	3	0.000	4	0.000	-0.121
Ag-5	3	0.027	3	0.461	0.313
Ag-6	4	0.144	3	0.664	0.399
Ag-7	5	0.468	2	1.999	1.410
Ag-8	5	0.473	3	1.502	0.908

irradiation, the formation processes of Ag NPs can reverse, and some of the Ag NPs reenter the bulk α - Ag_2WO_4 . This might be related to the fact that the energy barriers for movement out of the surface are very small, but also due to the presence of energy wells along the reaction coordinate, as can be seen from the NEB profiles (see figures 3 and 4).

α - Ag_2WO_4 crystals were irradiated during SEM experiments. Figure 5 shows the electrical resistance values as a function of the electron beam exposure time. The measurements show that after irradiation at 30 kV for 5 min the

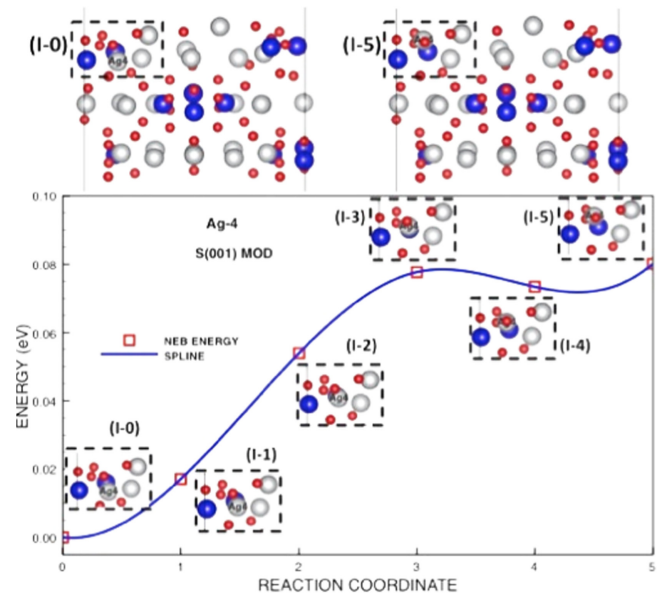


Figure 3. Structures and energy profile for the diffusion of the Ag-4 surface atom, obtained from NEB calculations. The top two images, labeled (I-0) and (I-5), depict the initial and final structures, respectively. Below, the energy profile along the reaction coordinate, which has a very small energy barrier of 0.08 eV. Insets of each of these structures (labeled I-0 to I-5) are shown adjacent to each energy value.

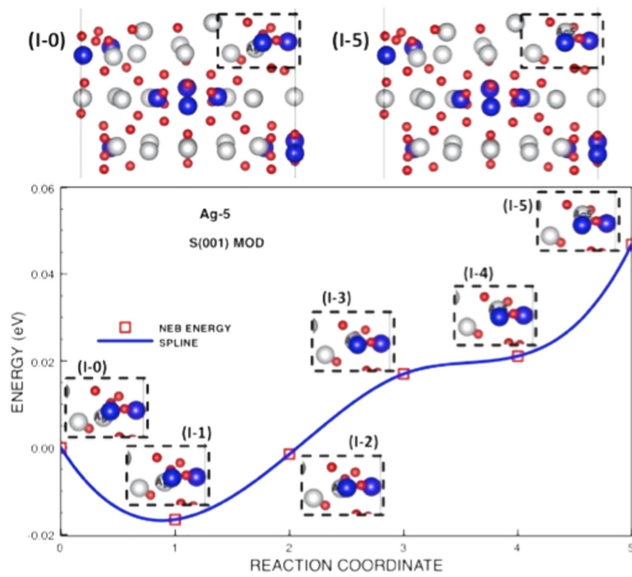


Figure 4. Structures and energy profile for Ag-5 surface atom, obtained from NEB calculations. The top two images labeled (I-0) and (I-5) depict the initial and final structures, respectively. Below, the energy profile along the reaction coordinate for the diffusion of Ag-5, showing its very small energy barrier of 0.05 eV. Insets of each of these structures (labeled I-0 to I-5) are shown adjacent to each energy value.

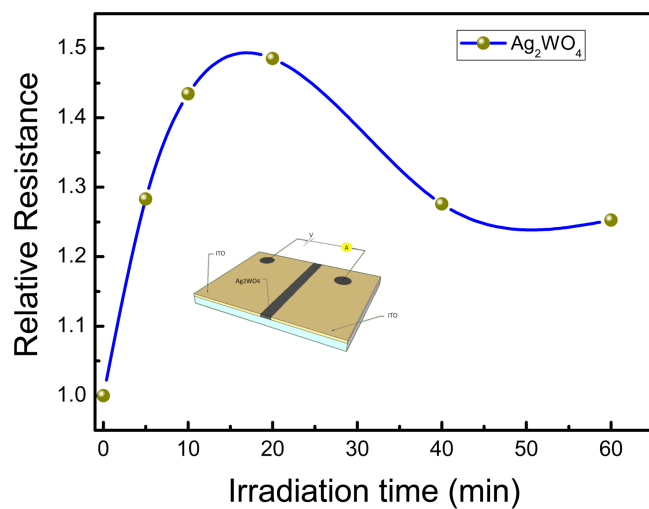


Figure 5. Changes in electrical resistance of α -Ag₂WO₄ nanoparticles as a function of the electron irradiation time. The experimental device is shown schematically in the inset.

resistance increased almost 30% with respect to the non-irradiated sample. As the exposure time increased, the resistance also increased, and after 20 min irradiation, the resistance increased by 50%. For longer irradiation times, a decrease in resistance was observed; even so, the resistance was still 30% greater than the initial resistance value.

It has been observed before [49, 50] that irradiation of α -Ag₂WO₄ NPs with electrons generates structural and electronic disorder, for example, increasing the electron-hole density. The increase in resistance (and consequent lower conductivity) is consistent with the appearance of Ag⁰ at the

nanoparticle surface, as observed by FE-SEM (figure 1 and supplementary material). This effect is called electrochemireduction (ECR). ECR increases with irradiation time, creating clusters of silver and silver vacancies [V'_{Ag}] that are responsible for the increase in electrical resistance. These clusters interact, giving rise to nanowires that emerge at the crystal surface. Simultaneously, there is the formation of a large number of [$V'_{Ag}Ox$] and holes, $h\bullet$. Finally, there is growth of Ag nanofilaments (as observed by FE-SEM, see figure 1). When the density of Ag filaments reaches a critical amount, in this case after irradiation for 20 min, these filaments contribute to a higher surface conductivity, and, consequently, lower the bulk resistance.

Conclusions

Finely focused electron beams in a transmission electron microscope or scanning electron microscope are routinely used to visualize nanomaterials. However, the electron irradiation can cause temporary or permanent changes in the surface or bulk structure of the specimen. Thus, we have the opportunity to observe new surface phenomena. In this paper, we have studied and described the physics behind the growth behavior of Ag nanoparticles on α -Ag₂WO₄ crystals exposed to electron beam irradiation. This growth phenomenon is discussed here based on physical models required to describe its unique features; in turn, this has allowed us to ask fundamental questions regarding the nature of Ag NPs growth mechanism provoked by electron excess and the effect of order-disorder on the different local CN of Ag atoms.

Theoretical results, connected with experimental evidence, reveal the Ag atoms that are likely, under the impact of the electron beam, to diffuse out of the surface to form the experimentally observed Ag NPs. DFT calculations have shown that there are surface Ag atoms with different CNs in the (001) surface. Furthermore, some of these are predisposed to diffuse out the surface following a pathway with a very low energy barrier (less than 0.1 eV). The energy profiles along the reaction coordinate have small wells that could explain the observed reversibility that sometimes occurs after the emergence of the Ag NPs. These calculations provide a deeper understanding of the important mechanisms involved in the electron irradiation of α -Ag₂WO₄ and the subsequent growth of Ag NPs.

Additionally, conductance measurements on the electron irradiated samples indicate that disorder increases in the bulk crystal upon irradiation due to the migration of Ag atoms out of the surface to form Ag clusters. Thus, Ag vacancies form in the bulk. Further irradiation causes some Ag metal atoms to return into the sample reducing the electrical resistance.

In summary, our model describes the experimental observables, and the computational work described here makes a connection between the chemical composition of the surface and its resulting electronic structure, as suggested by the electric transport property measurements. However, there undoubtedly remains considerable work to be done. DFT studies help to explain observations in the context of actual

atomistic changes on the crystal surface. Rapidly advancing computational methods allow for more realistic crystal models and let us re-evaluate long held theories about surface chemistry. A plasmonic model to explain surface excitonics is now more pertinent than ever.

Acknowledgments

The authors are grateful to Generalitat Valenciana (Spain) for *PrometeoII/2014/022* and *ACOMP/2014/270* projects, Ministerio de Economía y Competitividad (Spain), CTQ2012-36253-C03-02, and to the Spanish Brazilian Program (PHB2009-0065-PC), CAPES (203038 009607/2013-56 088/2013), INCTMN (2008/57872-1), FAPESP (2013/07296-2; 2012/14468-1; 2010/16970-0) and CNPq (147001/2013-7; 573636/2008-7) for financially supporting this research. Most of the calculations were performed using IFGW-UNICAMP computer facilities and the National Center for High Performance Computing in São Paulo (CEN-APAD-SP).

References

- [1] Williams D B and Carter C B 2009 *Transmission Electron Microscopy: A Textbook for Materials Science* (New York: Springer)
- [2] Fultz B and Howe J 2013 *Transmission Electron Microscopy and Diffractometry of Materials* (New York: Springer)
- [3] De Graef M 2003 *Introduction to Conventional Transmission Electron Microscopy* (New York: Cambridge University Press)
- [4] Egerton R F 2011 *Electron Energy-Loss Spectroscopy in the Electron Microscope* (New York: Springer)
- [5] Thomas J and Gemming T 2014 *Analytical Transmission Electron Microscopy: An Introduction for Operators* (New York: Springer)
- [6] Plemmons D A, Suri P K and Flannigan D J 2015 Probing structural and electronic dynamics with ultrafast electron microscopy *Chem. Mater.* **27** 3178–92
- [7] Xu Y M, Shi L, Zhang X T, Wong K and Li Q 2011 The electron beam irradiation damage on nanomaterials synthesized by hydrothermal and thermal evaporation methods—an example of ZnS nanostructures *Micron* **42** 290–8
- [8] Egerton R F, Li P and Malac M 2004 Radiation damage in the TEM and SEM *Micron* **35** 399–409
- [9] Evans J E, Jungjohann K L, Browning N D and Arslan I 2011 Controlled growth of nanoparticles from solution with in situ liquid transmission electron microscopy *Nano Lett.* **11** 2809–13
- [10] Zheng H, Smith R K, Jun Y, Kisielowski C, Dahmen U and Alivisatos A P 2009 Observation of single colloidal platinum nanocrystal growth trajectories *Science* **324** 1309–12
- [11] Noh K W, Liu Y, Sun L and Dillon S J 2012 Challenges associated with in situ TEM in environmental systems: the case of silver in aqueous solutions *Ultramicroscopy* **116** 34–8
- [12] Liao H-G, Cui L, Whitlam S and Zheng H 2012 Real-time imaging of Pt₃Fe nanorod growth in solution *Science* **336** 1011–4
- [13] Yuk J M, Park J, Ercius P, Kim K, Hellebusch D J, Crommie M F, Lee J Y, Zettl A and Alivisatos A P 2012 High-resolution EM of colloidal nanocrystal growth using graphene liquid cells *Science* **336** 61–4
- [14] Woehl T J, Evans J E, Arslan I, Ristenpart W D and Browning N D 2012 Direct in situ determination of the mechanisms controlling nanoparticle nucleation and growth *ACS Nano* **6** 8599–610
- [15] Latham A H and Williams M E 2008 Transmission electron microscope-induced structural evolution in amorphous Fe, Co, and Ni oxide nanoparticles *Langmuir* **24** 14195–202
- [16] Sood S, Kisslinger K and Gouma P 2014 Nanowire growth by an electron-beam-induced massive phase transformation *J. Am. Ceram. Soc.* **97** 3733–6
- [17] Yacaman M J, Gutierrez-Wing C, Miki M, Yang D, Piyakis K and Sacher E 2005 Surface diffusion and coalescence of mobile metal nanoparticles *J. Phys. Chem. B* **109** 9703–11
- [18] Latham A H, Wilson M J, Schiffer P and Williams M E 2006 TEM-induced structural evolution in amorphous Fe oxide nanoparticles *J. Am. Chem. Soc.* **128** 12632–3
- [19] Zhu X, Su J, Wu Y, Wang L and Wang Z 2014 Intriguing surface-extruded plastic flow of SiO_x amorphous nanowire as thermally induced by electron beam irradiation *Nanoscale* **6** 1499–507
- [20] Gao M, Zhang X, Yang B and Shen J 1994 A monolayer of PbI₂ nanoparticles adsorbed on MD-LB film *J. Chem. Soc.* **19** 2229–30
- [21] Wang Y, Feng Y, Chen Y, Mo F, Qian G, Yu D, Wang Y and Zhang X 2015 Morphological and structural evolution of WS₂ nanosheets irradiated with an electron beam *Phys. Chem. Chem. Phys.* **17** 2678–85
- [22] Warner J H 2008 Self-Assembly of ligand-free PbS nanocrystals into nanorods and their nanosculpturing by electron-beam irradiation *Adv. Mater.* **20** 784–7
- [23] Kim J, Cha S, Shin K, Jho J Y and Lee J C 2005 Synthesis of gold nanoparticles from gold(I)–alkanethiolate complexes with supramolecular structures through electron beam irradiation in TEM *J. Am. Chem. Soc.* **127** 9962–3
- [24] Wan D, Matteo M, Su W N, Xu L, Sun L T and Shen Y T 2013 The in situ TEM observation of rapid lithium encapsulation and release in LiCl nanoshells and nanotubes *Cryst. Eng. Commun.* **15** 7872–8
- [25] Liu Y Z, Lin X M, Sun Y G and Rajh T 2013 In situ visualization of self-assembly of charged gold nanoparticles *J. Am. Chem. Soc.* **135** 3764–7
- [26] Song X *et al* 2015 Formation of carbonized polystyrene sphere/hemisphere shell arrays by ion beam irradiation and subsequent annealing or chloroform treatment *Sci. Rep.* **5** 17529
- [27] Wijesundera D N, Rajapaksa I, Wang X, Liu J-R, Rusakovaa I and Chua W-K 2013 Ion beam engineered nano silver silicon substrates for surface enhanced Raman spectroscopy *J. Raman Spectrosc.* **44** 1014–7
- [28] Utke I and Götzhäuser A 2010 Small, minimally invasive, direct: electrons induce local reactions of adsorbed functional molecules on the nanoscale *Angew. Chem. Int. Ed. Engl.* **49** 9328–30
- [29] Böhrer E, Warneke J and Swiderek P 2013 Control of chemical reactions and synthesis by low-energy electrons *Chem. Soc. Rev.* **42** 9219–31
- [30] Wang H, Brandl D W, Nordlander P and Halas N J 2007 Plasmonic nanostructures: artificial molecules *Acc. Chem. Res.* **40** 53–62
- [31] Nelayah J, Kociak M, Stéphan O, Garcia de Abajo F J, Tencé M, Henrard L, Taverna D, Pastoriza-Santos I, Liz-Marzan L M and Colliex C 2007 Mapping surface plasmons on a single metallic nanoparticle *Nat. Phys.* **3** 348–53

- [32] Rang M, Jones A C, Zhou F, Li Z-Y, Wiley B J, Xia Y and Raschke M B 2008 Optical near-field mapping of plasmonic nanoparticles *Nano Lett.* **8** 3357–63
- [33] Alivisatos A P, Harris A L, Levinos N J, Steigerwald M L and Brus L E 1988 *J. Chem. Phys.* **89** 4001–11
- [34] Nosaka Y 1991 *J. Phys. Chem.* **95** 5054–8
- [35] Zhang J and Zhang L 2012 Nanostructures for surface plasmons *Adv. Opt. Photon.* **4** 157–321
- [36] Ringe E, McMahon J M, Sohn K, Cobley C, Xia Y, Huang J, Schatz G C, Marks L D and Van Duyne R P 2010 Unraveling the effects of size, composition, and substrate on the localized surface plasmon resonance frequency of gold and silver nanocubes: a systematic single particle approach *J. Phys. Chem. C* **114** 12511–6
- [37] Hutter E and Fendler J H 2004 Exploitation of localized surface plasmon resonance *Adv. Mater.* **16** 1685–706
- [38] Stewart M E, Anderton C R, Thompson L B, Maria J, Gray S K, Rogers J A and Nuzzo R G 2008 Nanostructured plasmonic sensors *Chem. Rev.* **108** 494–521
- [39] Kneipp K, Moskovits M and Kneipp H 2006 *Surface-Enhanced Raman Scattering* (Berlin: Springer)
- [40] Atwater H A and Polman A 2010 Plasmonics for improved photovoltaic devices *Nat. Mater.* **9** 205–13
- [41] Schimpf A M, Thakkar N, Gunthardt C E, Masiello D J and Gamelin D R 2014 Charge-tunable quantum plasmons in colloidal semiconductor nanocrystals *ACS Nano* **8** 1065–72
- [42] Faucheaux J A, Stanton A L D and Jain P K 2014 Plasmon resonances of semiconductor nanocrystals: physical principles and new opportunities *J. Phys. Chem. Lett.* **5** 976–85
- [43] Hartland G V 2011 Optical studies of dynamics in noble metal nanostructures *Chem. Rev.* **111** 3858–87
- [44] Kim J U, Cha S H and Shin K 2005 Synthesis of gold nanoparticles from gold(I)-alkanethiolate complexes with supramolecular structures through electron beam irradiation in TEM *J. Am. Chem. Soc.* **127** 9962–3
- [45] Sepulveda-Guzman S, Elizondo-Villarreal N and Ferrer D 2007 *J. Am. Chem. Soc.* **127** 9962–3
- [46] Rani M P, Kandikere R S, Srinath G, Bhat V and Manjunatha P 2010 Antibacterial potentiation of silver nanoparticles synthesized by electron beam irradiation *Int. J. Nanoparticles* **3** 53–64
- [47] Zheng H, Smith R K, Jun Y W, Kisielowski C, Dahmen U and Alivisatos A P 2009 Observation of single colloidal platinum nanocrystal growth trajectories *Science* **324** 1309–12
- [48] de Jonge N and Ross F M 2011 Electron microscopy of specimens in liquid *Nat. Nanotechnol.* **6** 695–704
- [49] Jungjohann K L, Bliznakov S, Sutter P W, Stach E A and Sutter E A 2013 In situ liquid cell electron microscopy of the solution growth of Au–Pd core–shell nanostructures *Nano Lett.* **13** 2964–70
- [50] Aabdin Z, Lu J, Zhu X, Anand U, Loh N D, Su H and Mirsaidov U 2014 Bonding pathways of gold nanocrystals in solution *Nano Lett.* **14** 6639–43
- [51] Longo E, Cavalcante L S, Volanti D P, Gouveia A F, Longo V M, Varela J A, Orlandi M O and Andres J 2013 Direct in situ observation of the electron-driven synthesis of Ag filaments on α -Ag₂WO₄ crystals *Sci. Rep.* **3** 1676
- [52] Andrés J *et al* 2014 Structural and electronic analysis of the atomic scale nucleation of Ag on α -Ag₂WO₄ induced by electron irradiation *Sci. Rep.* **5** 5391
- [53] Longo E, Volanti D P, Longo V M, Gracia L, Nogueira I C, Almeida M A P, Pinheiro A N, Ferrer M M, Cavalcante L S and Andres J 2014 Toward an understanding of the growth of Ag filaments on α -Ag₂WO₄ and their photoluminescent properties: a combined experimental and theoretical study *J. Phys. Chem. C* **118** 1229–39
- [54] da Silva Pereira W, Andrés J, Gracia L, San-Miguel M A, da Silva E Z, Longo E and Longo V M 2015 Elucidating the real-time Ag nanoparticle growth on α -Ag₂WO₄ during electron beam irradiation: experimental evidence and theoretical insights *Phys. Chem. Chem. Phys.* **17** 5352
- [55] Yuri J E C G, De Santana V B, Matos L, Henrique G, Cruvinel A P, Perrin C, Andrés J, Varela J A and Longo E 2014 Silver molybdate and silver tungstate nanocomposites with enhanced photoluminescence *Nanomaterials Nanotechnol.* **4** 22
- [56] da Silva L F, Catto A C, Avansi W Jr, Cavalcante L S, Andres J, Aguir K, Mastelaro V R and Longo E 2014 A novel ozone gas sensor based on onedimensional (1D) α -Ag₂WO₄ nanostructures *Nanoscale* **6** 4058–62
- [57] Longo V M *et al* 2014 Potentiated electron transference in α -Ag₂WO₄ microcrystals with Ag nanofilaments as microbial agent *J. Phys. Chem. A* **118** 5769–78
- [58] Alvarez R, Lemos P S, Andrés J and Longo E 2016 *Chem. Phys. Lett.* **644** 68–72
- [59] Andrés J, Ferrer M M, Gracia L, Beltran A, Longo V M, Cruvinel G H, Tranquilin R L and Longo E 2015 A combined experimental and theoretical study on the formation of Ag filaments on β -Ag₂MoO₄ induced by electron irradiation *Part. Part. Syst. Charact.* **32** 646–51
- [60] De Santana Y V B, Cardoso Gomes J E, Matos L, Cruvinel G H, Perrin C, Andres J, Varela J A and Longo E 2014 Silver molybdate and silver tungstate nanocomposites with enhanced photoluminescence *Nanomaterials Nanotechnol.* **4** 22
- [61] Botelho G, Sczancoski J C, Andres J, Gracia L and Longo E 2015 Experimental and theoretical study on the structure, optical properties, and growth of metallic silver nanostructures in Ag₃PO₄ *J. Phys. Chem. C* **119** 6293–306
- [62] Zhang R, Cui H, Yang X, Tang H, Liu H and Li Y 2012 Facile hydrothermal synthesis and photocatalytic activity of rod-like nanosized silver tungstate *Micro Nano Lett.* **7** 1285–8
- [63] Dutta D P, Singh A, Ballal A and Tyagi A K 2014 High adsorption capacity for cationic dye removal and antibacterial properties of sonochemically synthesized Ag₂WO₄ nanorods *Eur. J. Inorg. Chem.* **5724–32**
- [64] Chen H and Chu Y 2014 Photoactivity and stability of Ag₂WO₄ for organic degradation in aqueous suspensions *Appl. Surf. Sci.* **319** 319–23
- [65] Pan L, Li L and Chen Y H 2013 Synthesis and electrocatalytic properties of microsized Ag₂WO₄ and nanoscaled MWO₄ (M=Co, Mn) *J. Sol-Gel Sci. Technol.* **66** 330–6
- [66] Janáky C, Rajeshwar K, Tacconi N R D, Chanmanee W and Huda M N 2013 Tungsten-based oxide semiconductors for solar hydrogen generation *Catal. Today* **199** 53–64
- [67] Lin Z, Li J, Zheng Z, Yan J, Liu P, Wang C and Yang G 2015 Electronic reconstruction of α -Ag₂WO₄ nanorods for visible-light photocatalysis *ACS Nano* **9** 7256–65
- [68] Ng C H B and Fan W Y 2015 Uncovering metastable α -Ag₂MoO₄ phase under ambient conditions. overcoming high pressures by 2, 3-Bis(2-pyridyl)pyrazine doping *Cryst. Growth Des.* **15** 3032–7
- [69] Bao Z Y, Lei D Y, Dai J and Wua Y 2013 In situ and room-temperature synthesis of ultra-long Ag nanoparticles-decorated Ag molybdate nanowires as high-sensitivity SERS substrates *Appl. Surf. Sci.* **287** 404–10
- [70] Sreedevi A, Priyanka K P, Mary S R, Mohammed E M and Varghese T 2015 Nanophase -silver tungstate for potential applications in light emitting diodes and gate dielectrics *Adv. Sci. Eng. Med.* **7** 1–8
- [71] Vafaezadeh M and Hashemi M M 2015 One pot oxidative cleavage of cyclohexene to adipic acid using silver tungstate nano-rods in a Brønsted acidic ionic liquid *RSC Adv.* **5** 31298–302

Q2

- [72] Kresse G and Hafner J 1993 Ab initio molecular dynamics for liquid metals *Phys. Rev. B* **47** 558–61
- [73] Kresse G and Furthmüller J 1996 Efficiency of ab-initio total energy calculations for metals and semiconductors using a plane-wave basis set *Comput. Mater. Sci.* **6** 15–50
- [74] Kresse G and Furthmüller J 1996 Efficient iterative schemes for ab initio total-energy calculations using a plane-wave basis set *Phys. Rev. B* **54** 11169–86
- [75] Blöchl P E 1994 Projector augmented-wave method *Phys. Rev. B* **50** 17953
- [76] Kresse G and Joubert J 1999 From ultrasoft pseudopotentials to the projector augmented-wave method *Phys. Rev. B* **59** 1758
- [77] Blöchl P E, Jepsen O and Andersen O K 1994 Improved tetrahedron method for brillouin-zone integrations *Phys. Rev. B* **49** 16223
- [78] Perdew J P, Chevary J A, Vosko S H, Jackson K A, Pederson M R, Singh D J and Fiolhais C 1992 Atoms, molecules, solids, and surfaces: applications of the generalized gradient approximation for exchange and correlation *Phys. Rev. B* **46** 6671
- [79] Perdew J P, Burke K and Ernzerhof M 1996 Generalized gradient approximation made simple *Phys. Rev. Lett.* **77** 3865
- [80] Jonsson H, Mills G, Jacobsen K W and Berne B J 1998 *Classical and Quantum Dynamics in Condensed Phase Simulations* ed D Chandler *et al* (Singapore: World Scientific) p 385
- [81] Roca R A *et al* 2015 Facet-dependent photocatalytic and antibacterial properties of α -Ag₂WO₄ crystals: combining experimental data and theoretical insights *Catalysis Sci. Technol.* **5** 4091–107 and references therein

QUERY FORM

JOURNAL: Nanotechnology

AUTHOR: M A San-Miguel *et al*

TITLE: *In situ* growth of Ag nanoparticles on α -Ag₂WO₄ under electron irradiation: probing the physical principles

ARTICLE ID: nanoaa2090

The layout of this article has not yet been finalized. Therefore this proof may contain columns that are not fully balanced/matched or overlapping text in inline equations; these issues will be resolved once the final corrections have been incorporated.

SQ1

Please be aware that the colour figures in this article will only appear in colour in the online version. If you require colour in the printed journal and have not previously arranged it, please contact the Production Editor now.

We have been provided funding information for this article as below. Please confirm whether this information is correct. Coordenação de Aperfeiçoamento de Pessoal de Nível Superior: 009607/2013-56, 203038, 088/2013; FAPESP: 2010/16970-0, 2013/07296-2, 2012/14468-1.

Page 7

Q1

Please check the details for any journal references that do not have a link as they may contain some incorrect information.

Page 8

Q2

Please provide the volume number in reference [63].[↙](#)
